Thermodynamic properties and explosion energy analysis of carbon dioxide blasting systems

Bo Ke, Keping Zhou, Chaoshui Xu, Gaofeng Ren & Tingting Jiang

Check for updates

Thermodynamic properties and explosion energy analysis of carbon dioxide blasting systems

Bo Ke[a,b,c], Keping Zhou[b], Chaoshui Xu [d], Gaofeng Ren[a,c] and Tingting Jiang[a]

[a]School of Resources and Environmental Engineering, Wuhan University of Technology, Wuhan, People's Republic of China; [b]School of Resource and Safety Engineering, Central South University, Changsha, People's Republic of China; [c]Key Laboratory of Mineral Resources Processing and Environment of Hubei Province, Wuhan University of Technology, Wuhan, People's Republic of China; [d]School of Civil, Environmental and Mining Engineering, University of Adelaide, Adelaide, Australia

ABSTRACT

A carbon dioxide (CO_2) blasting system is a reusable non-explosive blasting product that can be used in many engineering applications. To investigate the influences of thermodynamic properties of liquid CO_2 and its explosion energy during the phase transition, the pressure within the blasting tube was measured in a laboratory for a liquid CO_2 blasting system. Based on the measured pressure curve, the CO_2 blasting process can be divided into three stages: pressure rising stage, pressure release stage and pressure recovery stage. The evolutions of temperature, pressure, phase transition and explosion energy of the CO_2 blasting system were analysed in detail in this work. The results show that the variation rate of temperature increases as the initial density of CO_2 decreases. The effect of initial CO_2 density on its isochoric heat capacity is also significant as the lower the initial density, the higher the peak specific heat capacity at the critical temperature. Based on the Span and Wagner CO_2 equation of state and the thermodynamics of explosions, a method is proposed to calculate the explosion energy of CO_2 blasting systems. This method produces more accurate and realistic results.

Physical constants for carbon dioxide used in this research

R Specific gas constant:
$R = R_m/M = (0.1889241 \pm 0.0000116)$ kJ/(kg K);

T_c Critical temperature: $T_c = (304.128 \pm 0.015)$ K;

p_c Critical pressure: $p_c = (7.377 \pm 0.0030)$ MPa;

ρ_c Critical density: $\rho_c = (467.6 \pm 0.6)$ kg/m³;

T_0 Reference temperature: $T_0 = 298.15$ K;

p_0 Reference pressure: $p_0 = 0.101\,325$ MPa

s_0^o Reference entropy in the ideal gas state at T_0, p_0: $s_0^o = 0$ kJ/(kg K)

Introduction

Increasing safety and environmental concerns in mining and related industries have led to the investigation of new methods of excavation that can improve safety (e.g. in coal mining) and reduce impacts on the surrounding environment, particularly when the activity is within the proximity of residential areas, cultural heritage or areas of specific interest. Consequently, there is an escalating number of products on the market claiming beneficial performances such as reduction in noise, ground vibration, dust and flyrocks (Caldwell 2004). One of the promising and non-explosive concepts that warrant in-depth evaluation as a tool for rock breakage is the 'penetrating cone fracture' (PCF) method (Singh 1998). Carbon dioxide blasting system (Rustan et al. 2010) is one of the non-explosive technologies within this category. The carbon dioxide blasting system, known as the Cardox system, is based on the idea of converting liquid (supercritical) carbon dioxide to high-pressure carbon dioxide gases by ignition (Caldwell 2004).

The Cardox system consists of a high-strength, reusable steel tube filled with liquid carbon dioxide, a chemical energiser/Cardox safety heater and a rupture disc. When the Cardox tube is ignited, the liquid carbon dioxide is almost instantaneously converted to gases (Caldwell 2004), which is then released from the tube and expands through micro-cracks and fractures within the rock, causing it to break in tension, rather than in compression as with normal explosives. It is this tensile rock breakage mechanism that results in the characteristics of reduced noise, ground vibration, and flyrocks, as less energy is required to break the rock in this mechanism and therefore much less residual energy is available after rock breakage to cause problems. Pressure released from the gaseous CO_2 can be regulated between 1200 and 2800 bar by using different rupture disks with different thickness. Figure 1 shows a schematic diagram of the components which make up the CO_2 blasting cartridge. The chemical energiser is

CONTACT Chaoshui Xu ✉ chaoshui.xu@adelaide.edu.au School of Civil, Environmental and Mining Engineering, University of Adelaide, Adelaide, SA 5005, Australia; Gaofeng Ren rgfwhut@163.com School of Resources and Environmental Engineering, Wuhan University of Technology, Wuhan, Hubei 430070, People's Republic of China; Key Laboratory of Mineral Resources Processing and Environment of Hubei Province, Wuhan University of Technology, Wuhan, Hubei 430070, People's Republic of China
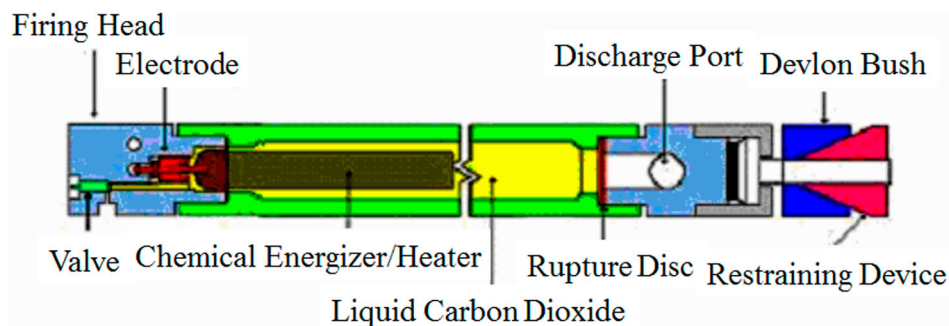
Figure 1. Schematic diagram of a Cardox (Caldwell 2004) system. Images are available in colour online.

activated by a small electrical charge which triggers the explosion.

In the 1930s, the Cardox system was first used as an alternative to explosives in coal mines. It became extensively used during the early 1950s, when 2.5 million shots were fired annually (Lu et al. 2015). The majority of these applications in coal mines were in the USA (Weir and Edwards 1928), Germany (Gaertner 1952), Britain (Wilson 1954) and France (Clairet 1952). Due to the rapid development of coal mining technologies and fully mechanised mining machines, the Cardox system is rarely used today in coal mining. Over the past twenty years, with increasing concerns about coal mining safety and chemical explosives control, the advantages of the Cardox system have raised its applicability in some coal mines for improving coal seam gas drainage (Zou and Panawalage 2001; Pantovic et al. 2002; Vidanovic et al. 2011; Zhang et al. 2015).

Other important applications of the Cardox system include environment-friendly blasting (Ribovich and Watson 1973), frozen ground blasting (Wood 1973), icebreaking (Mellor 1980), concrete removal (Campbell Sr 1982), urban underground construction (Pesch and Robertson 2007), rock breakage in forests (Parsakhoo and Lotfalian 2009), highway construction under freezing conditions in cold regions (Parsakhoo et al. 2010) and controlled blasting (Bajpayee et al. 2004; Durga and Swetha 2015). The Cardox system also has many specific applications in deep-sea excavation, tunnelling, shaft sinking, trenching and excavation (Caldwell 2004).

Although this technique has achieved increasing use as a non-explosive blasting technology, the blasting dynamics of Cardox attracts little attention in the scientific literature. Building on the fundamental work of Hawkes (1958) on the design and characteristics of the Cardox blasting system, other researchers have extended the work to investigate the speed at which the strata breaks up and the pressure which acts on the fracture planes during the blast. For the energy associated with the pressurised carbon dioxide gas, the formulas developed by Lu et al. (2015) indicated that the energy is a function of the velocity of releasing gas from the nozzle, the peak pressure in

the Cardox tube, the gas density and the pressure outside the Cardox tube. However, very little attention was paid to the influences of the thermodynamic properties (such as density, internal pressure and temperature) of liquid carbon dioxide on the explosion of energy during the phase transition within the Cardox tube.

In this work, an experimental system of CO_2 blasting was built to examine the pressure change within the Cardox tube during the CO_2 blasting process. Published real equations of state for CO_2 were reviewed and an equation of state (EOS) in the form of a fundamental equation explicit in the Helmholtz free energy for the CO_2 blasting system is proposed. Using the real EOS for CO_2 and the measured pressure, the thermodynamic properties such as temperature, isochoric heat capacity and Helmholtz free energy in the tube were obtained. The evolutions of the temperature, pressure, phase transition and explosion energy of the CO_2 blasting system were then analysed in detail.

Experimental methodology

The study of thermodynamic properties and phase transition of CO_2 within the Cardox tube is of critical importance to the understanding of the speed of fluid release, the energy of the explosion and the pressure exerting on the rock. CO_2 blasting is a phase transition process involving the exchange of heat and the accumulation of energy. The two key factors that affect the thermodynamic properties of CO_2 are temperature and initial liquid density. The initial density can be calculated by the mass difference before and after filling the tube. The temperature in the tube is difficult to measure directly in the experiment because CO_2 blasting is an extremely fast process (it only lasts milliseconds). However, the pressure within the tube can be recorded during the blasting process and the relationship between temperature and time can be established with the help of the real EOS for CO_2 and the measured pressure data. Consequently, the thermodynamic properties and phase transition of the CO_2 blasting system can be analysed.

Figure 2 shows the test system used in this research. Pressure transducer A placed in the tube wall was used
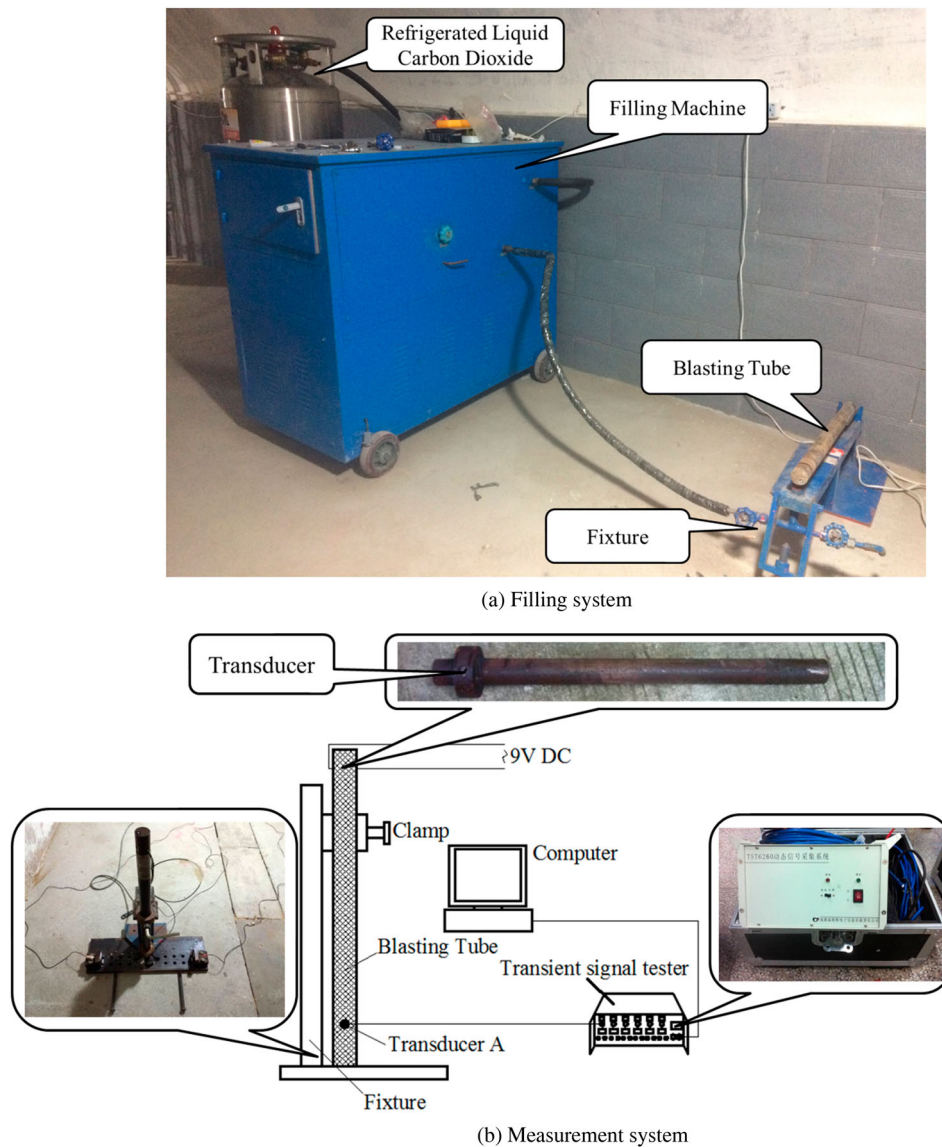
Figure 2. Schematic diagram of CO_2 blasting tube filling and testing system. (a) Filling system. (b) Measurement system. Images are available in colour online.

to measure the internal pressure within the tube. The primary components of the test system include the following:

(1) The CO_2 filling system (Figure 2(a)) which includes a storage tank for liquid CO_2, the liquid filling machine, the CO_2 blasting tube and the fixing device used for filling the CO_2. The filling machine consists of a main control switch, a control panel and an operation platform. The main switch controls the opening and closing of the whole liquid CO_2 filling system. The control panel is used to adjust the filling pressure. The fixing device is used to connect the blasting tube securely to the filling system. The dimensions of the blasting tube used in our tests are 700 mm × Φ45 mm.

(2) The dynamic pressure measurement system (Figure 2(b)) which includes the fixture, the computer, the TST6200 transient signal recorder and the piezoelectric pressure sensors with the measuring range of 0–250 MPa. The system is used to record the pressure signals within the blasting tube during the blasting process. The data sampling frequency is 50 kHz.

All the explosion tests were carried out in a specially built air-raid shelter with an average temperature of 18°C and an average humidity of 89%. For each test, before filling, the entire filling system and the blasting tube were cooled down through 2–3 filling and exhaust cycles. The blasting tube was then charged with the filling pressure of 9 MPa. The filled basting tube was placed on the fixture of the system, ready for testing (Figure 2(b)).

Results and discussions

Phase diagrams of carbon dioxide

Generally speaking, the error in the state equation of an ideal gas is greater when the pressure is high or the gas
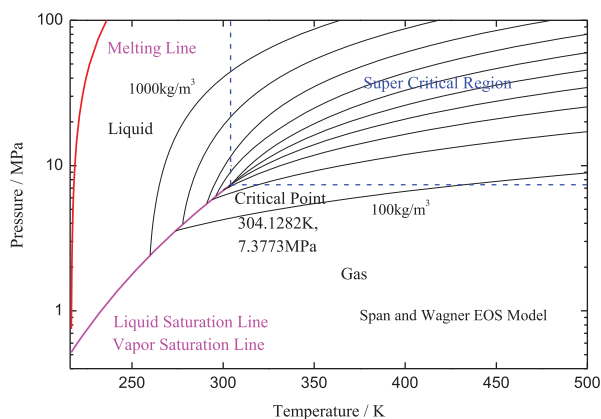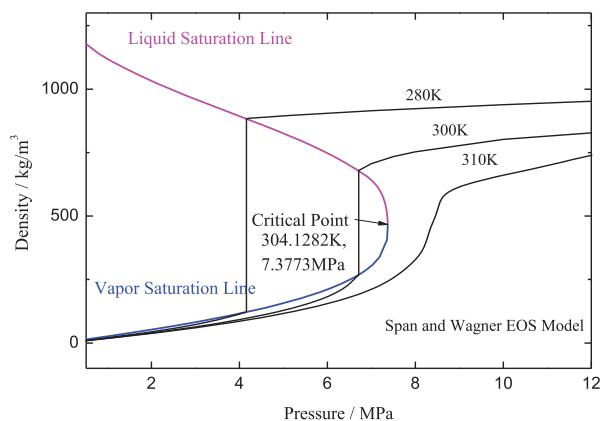
Figure 3. Carbon dioxide p–T phase diagram. Images are available in colour online.

is close to its critical point (Mizuno et al. 2002; Calvignac et al. 2010). The Span and Wagner EOS is generally regarded as the preferred method for calculating equilibrium thermodynamic properties of CO_2 (Span and Wagner 1996; Elshahomi 2015)

Figure 3 shows the phase diagram of CO_2. Based on the pressure–temperature phase diagram, two different phase states exist, namely liquid phase and gas phase. Both phases will disappear and CO_2 will turn into the supercritical fluid with a single phase state when the temperature and pressure exceed the critical point (304.1 K, 7.38 MPa). In the region of the supercritical state of CO_2, the pressure increases with the density of CO_2.

Figure 4 shows the phase diagram of density–pressure of CO_2. When the temperature is lower than the critical temperature, the gas will be compressed into a high-density liquid as the pressure increases, which is illustrated by the continuous vertical lines shown in the figure. In this case, the high-density liquid and the low-density gas are included in the system which reaches the balanced state. The density of gas will increase but the density of liquid will decrease as the temperature increases at the same pressure. CO_2 turns into a homogeneous phase when the values of

temperature and pressure exceed the critical point where the density of gas and liquid becomes identical.
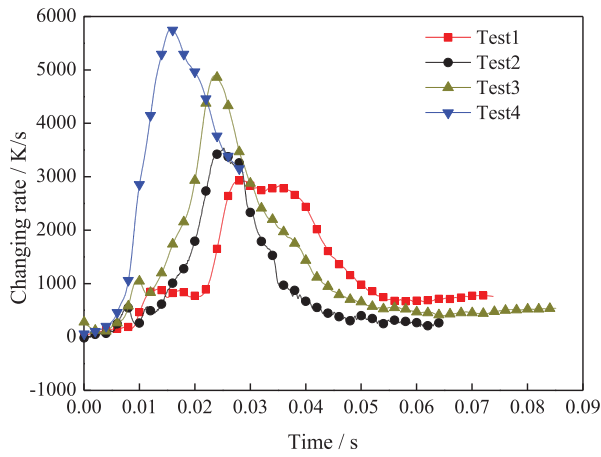
Temperature in the tube

When the heater within the tube is activated, the heat is transmitted to the liquid CO_2, causing both the temperature and the internal pressure of the blasting tube to increase until the rupture disc is destroyed. The variation of the internal pressure within the tube throughout the whole blasting process is recorded by the transient signal recording instrument. Figure 5 shows the relationship between the internal pressure and time before the rupture disc was destroyed for four experiments at the same filling pressure but with different rupture disc yield pressures, resulting in different peak pressures in the tube. Based on the Span and Wagner EOS of CO_2 and the recorded pressure data (Figure 5), the relationship between the temperature within the tube and time can be obtained, which is shown in Figure 6. The corresponding rate of change in temperature is shown in Figure 7. Table 1 lists the CO_2 mass, density, initial and peak temperature within the tube for the four tests shown in Figure 6.
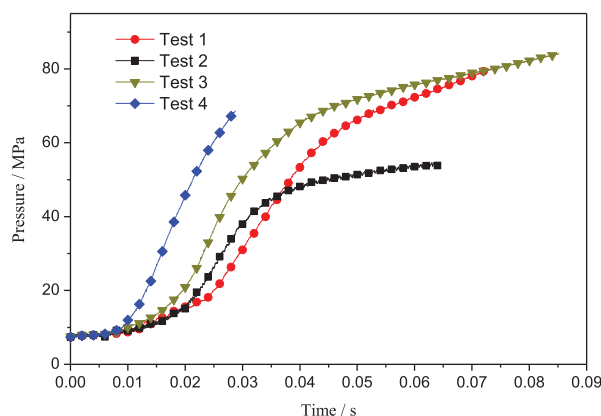
Figure 5. The variation of pressure within the tube before the rupture disc breaks. Images are available in colour online.

Figure 4. Carbon dioxide ρ–p phase diagram. Images are available in colour online.
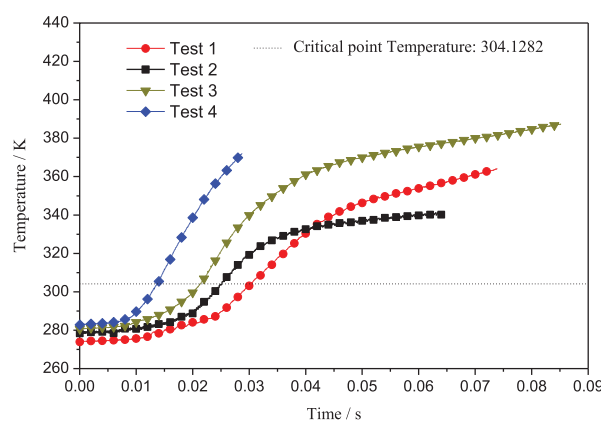
Figure 6. The variation of temperature within the tube before the rupture disc breaks. Images are available in colour online.

Figure 7. The rate of change in temperature within the tube before the rupture disc breaks. Images are available in colour online.

The pressure and temperature curves have the same variation patterns (Figures 5 and 6). The rates of increment in temperature decrease with the increase in initial density (Figure 7) and the temperature rises faster when the initial temperature is higher. This is due to the fact that the heat of evaporation per unit of liquid is related to the vaporisation temperature. The liquid molecules have higher kinetic energy with the increase in temperature. The difference between gas phase and liquid phase gradually reduces and a little energy can transform the liquid phase into the gas phase. The higher the initial temperature, the less the heat of evaporation required. When the CO_2 is at its critical state, there is no difference between the gas phase and the liquid phase. The initial temperature of Test 4 is the highest, while its density is the lowest, so the heat needed to vaporise before the critical state for this case is the least compared with other cases.

In summary, the initial temperature is an important factor for the CO_2 blasting system, the lower the initial temperature, the better the filling. The state of the CO_2 blasting system at a lower temperature can improve the efficiency of the filling process. The rate of change in temperature increases with the decrease in the initial density of CO_2. The higher the initial temperature, the faster the vaporisation temperature increases. The curve of temperature change appears initially as a concave exponential curve, then increases rapidly in a linear fashion, followed eventually by a gentle increase. The difference in the yield pressure of the rupture disc results in different peak pressure and temperature in the tube.

From Figure 6, it can be seen that the curves of temperature vs time rise slowly first, then rapidly following approximately a straight-line and gently at the final stage. According to the law of thermodynamics, the temperature increases because of absorbing heat in the process. The heat absorbed to increase the temperature of the system by 1 K is proportional to the specific isochoric heat capacity and density. Figure 8 shows the specific isochoric heat capacity c_v and its rate of change calculated by the Span and Wagner EOS. Four stages can be recognised in the sinusoidal curve of c_v: (1) a slow decrease to the first minimum;

Table 1. The mass, density, initial and peak temperature of carbon dioxide of four tests.

Number	Before filing (kg)	After filing (kg)	CO_2 weight (kg)	Volume (m³)	Density (kg/m³)	Initial temperature (K)	Peak temperature (K)
1	5.319	5.710	0.391	0.00041	953.49	273.89	364.19
2	5.320	5.701	0.380	0.00041	927.91	278.36	341.42
3	5.319	5.694	0.375	0.00041	915.00	280.61	387.46
4	5.320	5.686	0.369	0.00041	900.00	282.77	371.96
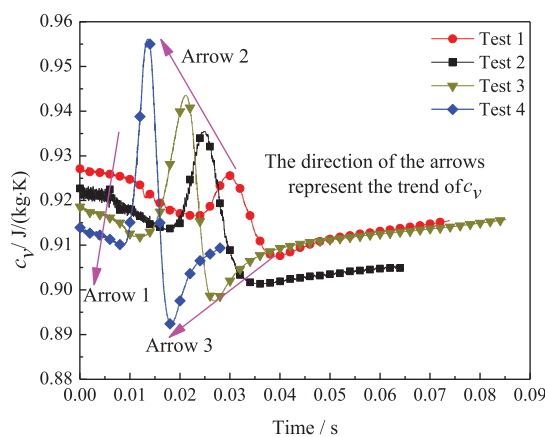
a) Specific isochoric heat capacity
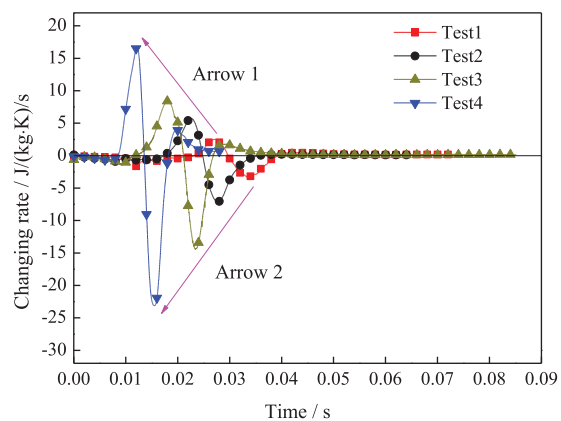
b) Rates of change in specific isochoric heat capacity

Figure 8. Specific isochoric heat capacity and its rates of change. (a) Specific isochoric heat capacity. (b) Rates of change in specific isochoric heat capacity. Images are available in colour online.

(2) a steep rise to the maximum; (3) a steep drop following the maximum decreasing slope; and (4) a slow increase from the second minimum. The variations of temperature can also be divided into four stages corresponding to the characteristics of c_v and its rate of change. The comparisons of temperature T, c_v and their rates of change are shown in Figure 9, where the black dashed lines are indicators of boundaries between different stages.

Stage 1: As shown in Figure 8(a), the value of c_v decreases as the density decreases (arrow 1 indicates the direction). From Figure 9, c_v decreases slowly to the first minimum, and the rates of change of c_v are negative. The curves of changing rates of c_v first have a slow decrease to the minimum and then increase to the value of zero. The temperature has a slow increase, and its rate of change gradually increases. The absorbed heat leads to an increase in temperature, but the increase is slow because the rate of the increment in internal energy is suppressed by the diminution of c_v.

Stage 2: c_v increases rapidly to its peak as the temperature rises fast. The lower the initial density, the higher the maximum value of c_v (arrow 2 in Figure 8 (a) indicates the direction). The rates of change of c_v are positive. The curves of changing rates of c_v first rise rapidly up to the maximum and then quickly drop back to the value of zero. The rate of change

increases as the initial density decreases (arrow 1 in Figure 8(b) indicates the direction). The rate of change in temperature keeps increasing in this stage, apart from Test 1 where it reaches its maximum value before the end of this stage. The rapid increases of c_v and its rate of change in this stage will further accelerate the rate of increase in the internal energy of the system. As a consequence, the temperature and its rate of change also increase rapidly. Note that the peak of c_v corresponds to the critical temperature point of CO_2.

Stage 3: From this stage, the CO_2 becomes a supercritical fluid. c_v decreases until it reaches the second minimum. The lower the initial density, the higher the maximum value of c_v (arrow 3 in Figure 8(a) indicates the direction). The rates of change of c_v are negative. The curves of changing rates of c_v decrease rapidly to the minimum and then quickly return to the value of zero. The rates of change of c_v increase as the initial density decreases (arrow 2 in Figure 8(b) indicates the direction).

The rates of change of temperature in this stage decrease quickly after they reach their maximum values. Even the temperature still increases quickly, such as in Stage 2, the rates of change in temperature begin gradually to slow down as shown in Figure 9. This is because c_v is at a high value initially within this stage and therefore the temperature still increases
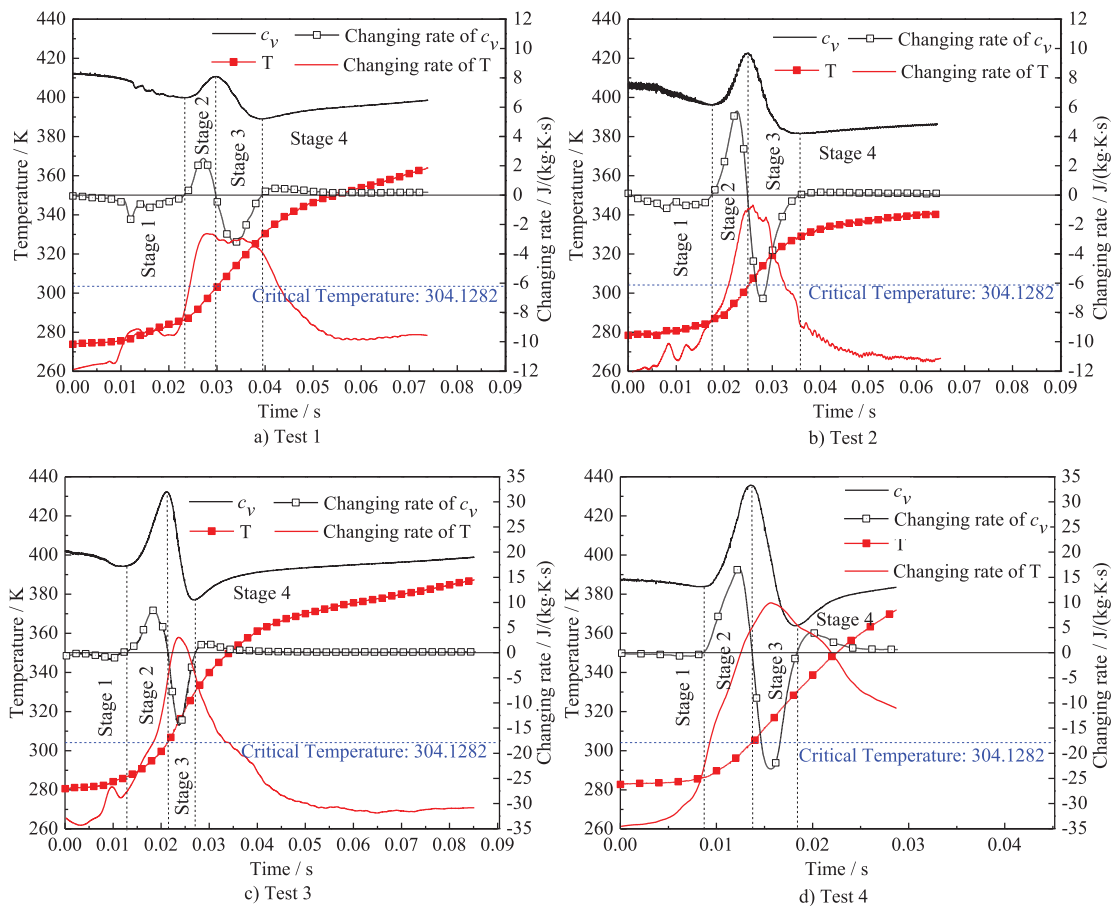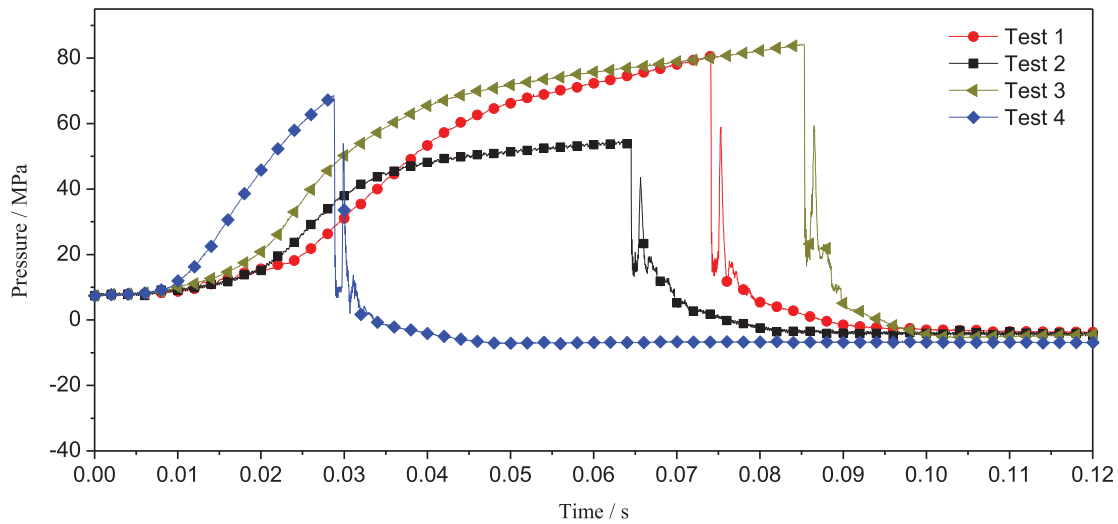

Figure 9. Comparisons of temperature T, c_v and their rates of change. Images are available in colour online.

Figure 10. Pressure vs. time within the blasting tube. Images are available in colour online.

at a high rate. Later in this stage c_v is at a low value, which suppresses the rates of change in temperature and makes them to decrease quickly.

Stage 4: c_v increases again from the second minimum, but the rates of change in c_v are different for different tests. For Test 1 and 2 (Figure 9(a) and (b)), the values of c_v increase slowly, and the curves of changing rates are close to a horizontal line. However, for Test 3 and 4 (Figure 9(c) and (d)), the values of c_v increase rapidly initially from its minimum and then slowly increase. Consequently, the rates of change curves increase to the maximum then slowly decrease and finally approach a horizontal line. In other words, the temperatures of Tests 1 and 2 increase at a slower pace compared with the temperatures of Tests 3 and 4, which increase rapidly initially from the minimum value, followed by a slow increase similar to Tests 1 and 2.

From the above analysis, the effect of the initial density of CO_2 on specific isochoric heat capacity c_v appears to be significant. The lower the initial density, the larger the peak specific isochoric heat capacity at the critical temperature. Based on the variation of the specific isochoric heat capacity, the curve of temperature variations can be divided into four stages. The specific isochoric heat capacity and its rate of change determine the increasing rate of temperature in the system.

Pressure evolutions within the blasting tube

After the heater is activated, transducer A records the changes in pressure within the blasting tube through the whole blasting process. The curves recorded for the four experiments conducted are shown in Figure10.

As an example of showing the characteristics of the pressure profile, a detailed analysis is done for the curve for Test 1. As shown in Figure 11, the pressure in the blasting tube increases rapidly after the heater is activated. The rupture disc is destroyed when the pressure reaches the yield stress of the disc (point B in Figure 11). High-pressure fluid releases rapidly and the pressure in the tube decreases sharply. The pressure curve of the
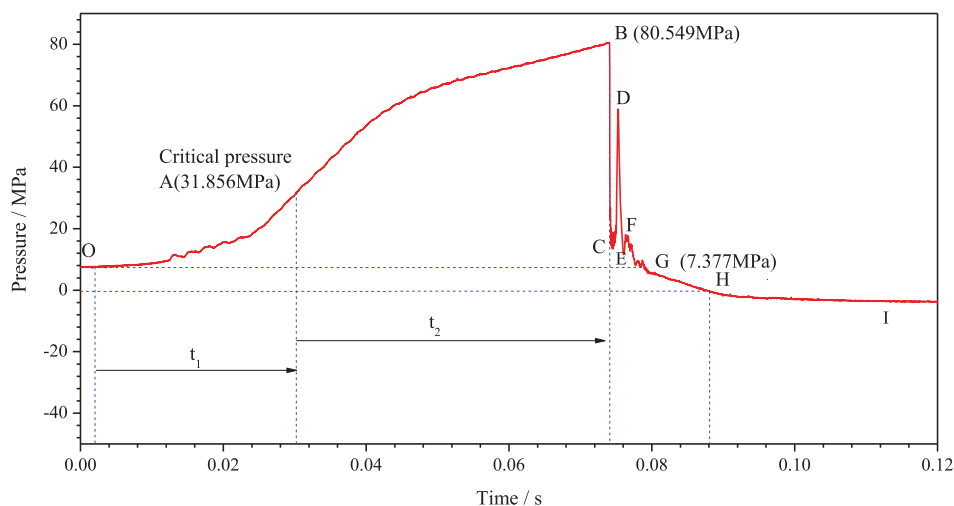
Figure 11. Pressure graph for Test 1. Images are available in colour online.
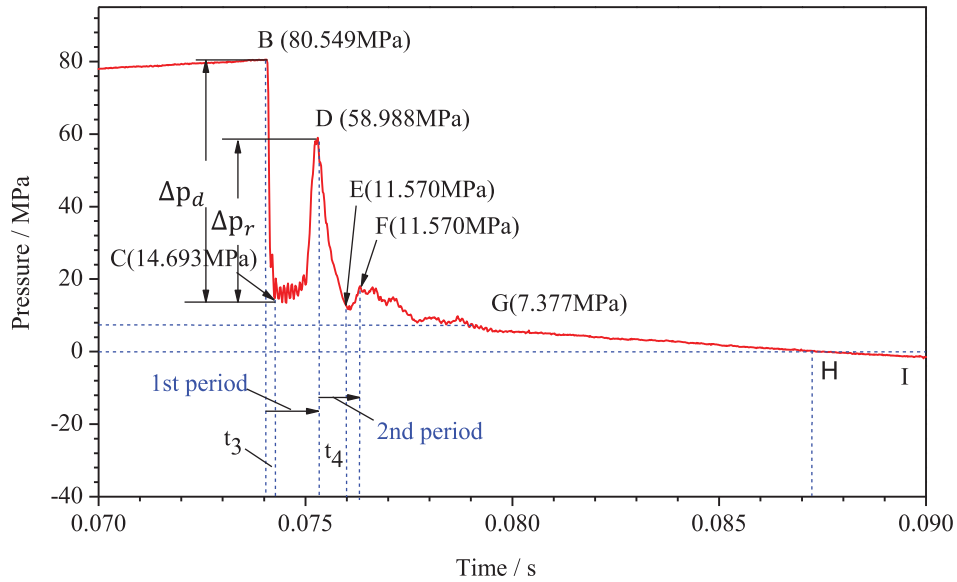
Figure 12. Pressure relief graph for Test 1. Images are available in colour online.

CO_2 blasting process can be divided into three stages (Figure 11).

(1) Pressure rise stage ($t_1 + t_2$)

In this stage, the liquid CO_2 absorbs heat and the pressure in the tube increases before the rupture disc is destroyed. It is well-known that the pressure of liquid sealed in a container is caused by the collision between liquid molecules in random motion and the wall of the container. The higher the temperature, the stronger the molecular movement, hence pressure is inherently related to temperature. As the number of molecules colliding with the wall increase, so does the macroscopical pressure exerted on the wall. The relationship between pressure and temperature is linear thus the variation features of the pressure curve and temperature curve should be the same. For the example shown in Figure 11, the time interval (t_1) of OA is 0.028 s, the pressure at point A is 31.856 MPa, which is the critical pressure of CO_2. After this point, the liquid in the blasting tube enters the supercritical state until the pressure reaches its peak at point B. The time interval (t_2) of AB for the example is 0.044 s.

(2) Pressure release stage

As shown in Figure 12, explosion behaviour is observed at this stage with an instantaneous depressurisation within the tube as the rupture disc fails, leading to a decompression wave. In the first period, the decompression wave travels at the local sound velocity of 805.32 m/s from the orifice to the closed tube end. The pressure drops rapidly when the decompression wave arrives at the transducer. The pressure falls from the maximum (B, 80.549 MPa) in front of the depressurisation wave to the minimum (C, 14.693 MPa) behind the depressurisation wave by the time of t_3 (0.00022 s), with the pressure drop amplitude at Δp_d. In such a situation, when the decompression wave arrives, the CO_2 inside the tube is at a temperature (peak temperature, 364.19 K) above the boiling point, which causes the initial phase to be turned rapidly into the superheated state. Following the pressure undershoot, the extremely rapid growth of vapour bubbles (Abbasi and Abbasi 2007; Guo et al. 2016) in the superheated state causes the pressure to recover to the second maximum pressure point (D, 58.988 MPa), and the pressure rebound amplitude is Δp_r. Afterwards, the reflected wave propagates from the tube end towards the orifice, causing the pressure to drop to the second minimum pressure point (E, 11.570 MPa) by the time t_4 (0.00104 s), whereafter it rebounds to the third maximum pressure point (F, 18.087 MPa). With the decompression wave propagating and reflecting repeatedly, Δp_d and Δp_r reduce gradually until the pressure drop and rebound inside the tube become insignificant after the critical pressure point (G, 7.377 MPa). After this point, the pressure decreases gradually in an approximately linear fashion.

(3) Pressure recovery stage

This stage begins with the appearance of negative pressure in the tube and lasts until the air pressure returns to normal atmospheric pressure. The time it takes for this process to complete is about 0.2–0.3 s.

Based on the analyses discussed above, the pressure and time at each critical point of the different stages of the pressure curve can be obtained, as shown in Table 2, for the example shown in Figures 11 and 12. The critical pressure value (A) and time (t_1) decrease as the initial density decreases. The pressure values are all

Table 2. The pressure and time for each inflection point of different stages.

Number	Density (kg/m³)	Peak temperature (K)	Speed of sound (m/s)	Pressure (MPa)						Time (ms)			
				A	B	C	D	E	F	t_1	t_2	t_3	t_4
Test 1	953.49	364.19	805.32	31.856	80.549	14.693	58.988	11.570	18.087	28.30	43.70	0.22	1.04
Test 2	927.91	341.42	720.44	26.486	54.731	15.211	43.620	14.130	19.475	25.16	39.22	0.28	0.98
Test 3	915.00	387.46	775.46	24.120	84.206	25.136	59.401	21.232	23.124	21.38	63.76	0.26	1.08
Test 4	900.00	371.96	726.08	21.645	68.642	16.140	53.928	13.267	16.420	13.72	15.00	0.18	1.00

greater than the CO_2 critical pressure of 7.377 MPa. The peak value is related to the yield pressure of the rupture disc. The time durations of the rising pressure stage for four tests are 72, 64.38, 85.14 and 28.72 ms, respectively. The rate at which the pressure drops reflects the work done by the pressurised liquid. As shown in Figure 11, in the first period, the release times (t_3) are 0.22, 0.28, 0.26 and 0.18 ms, respectively, which are close to the energy release time of explosive blasting. The corresponding pressure drop rate of the four experiments are 299.34, 141.14, 227.19, 291.68 GPa/s. In the second period, the release times (t_4) for the four tests are 1.04, 0.98, 1.08 and 1.00 ms, respectively. The corresponding pressure drop rates are 45.59, 30.09, 35.34, 40.66 GPa/s, which are only 15.23%, 21.32%, 15.56%, 13.94% respectively of the values obtained in the first period. On the other hand, the pressure values at pressure point D are 73.23%, 79.70%, 70.54% and 78.57% of those at pressure point B.

In terms of the mechanism of the pressure response in the tube, the process involves the complex theory of multiphase fluid dynamics (Guo et al. 2016), as shown in Figure 13. When the heater is activated, the temperature of CO_2 increases rapidly due to the heat absorption, as does the pressure. When the temperature and pressure of CO_2 reach their critical values, the CO_2 in the tube enters its supercritical state. When the internal pressure exceeds the strength of the rupture disc, the disc breaks, causing the high-pressure supercritical CO_2 to be released from the tube as a jet flow. The internal pressure along the tube drops quickly as the front of the decompression wave moves at the speed of sound. The supercritical CO_2 is brought into a superheated state due to the rapid depressurisation and the temperature above the atmospheric pressure boiling point. As a consequence, vapour bubbles grow rapidly and the constraint on the expanding two-phase system (by physical, acoustic or inertial means) results in the re-pressurisation of the system, which can bring the pressure back to nearly the original tube pressure. This process is followed by the collapse of bubbles, resulting in the formation of an intensified powerful fluid shock wave. The entire process is termed the Boiling Liquid Expanding Vapour Explosion (BLEVE) (Abbasi and Abbasi 2007), which clearly indicates that the CO_2 blasting process is not just a simple CO_2 vaporisation process.
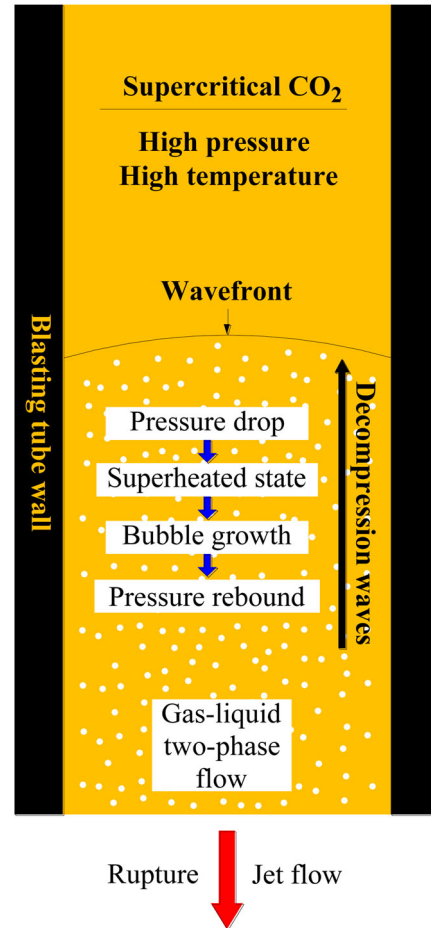
Figure 13. Schematic diagram of pressure response process of CO_2 blasting. Images are available in colour online.

Energy of explosion

Helmholtz free energy function for the explosion energy

The total amount of energy transferred from an explosive to the blast wave is the explosion energy, which is a key quantity in the study of blasting. Theoretically, the explosion energy could be calculated from the volume, V, of explosion expansion over its range of pressure, P, by evaluating the integral $\int_1^2 p\,dV$; that is, by finding the expansion work of the system (Kinney and Graham 2013). However, the evaluation of this integral could be difficult because it requires knowledge of the initial conditions of the explosion, plus the pressure-volume relationships for the gas the temperature of which is changing. An alternative to this evaluation is an overall thermodynamic analysis made directly in terms of terminal values. Such an analysis indicates that the pertinent item is the Helmholtz free energy function, A,

which is a point function defined in terms of the internal energy (E), the temperature (T) and entropy (s) as

$$A = E - Ts \tag{1}$$

This is analogous to the more common Gibbs free energy function, $G = E + PV - TS$. The explosion energy then is the decreased Helmholtz free energy function (Kinney and Graham 2013).

$$\text{Energy of explosion} = \int_1^2 p\,\mathrm{d}V \cong -\Delta A \cong -\Delta E + T\Delta s \tag{2}$$

A common formula for the explosion energy of the CO₂ blasting

This section presents a formula for the calculation of the explosion energy based on the ideal gas EOS in Kinney and Graham (2013). This common formula is widely used to assess the explosion energy of CO_2 blasting in coal seam gas drainage (Lu et al. 2015).

The essence of CO_2 blasting is the expansion of a compressed gas and hence there is no entropy in the explosion (Kinney and Graham 2013). Under such a circumstance the explosion energy equals the decrease of internal energy of the system, $-\Delta E$. The energy of the carbon dioxide explosion in the steel tube can be written as (Kinney and Graham 2013; Lu et al. 2015)

$$\text{Energy of explosion} = -\Delta E = \frac{1}{k-1} RT_1(1 - T_2/T_1)$$
$$= \frac{1}{k-1} p_1 V_1[1 - (p_2/p_1)^{(k-1)/k}] \tag{3}$$

where p_1 is the pressure of compressed carbon dioxide before the explosion in the steel tube, which is the peak pressure; V_1 is the volume of the steel tube; p_2 is the ambient pressure into which the carbon dioxide gas expands, which is the atmospheric pressure of 0.103 MPa, and k is the heat capacity ratio of carbon dioxide, which is 1.295.

The calculated explosion energies for the four blasting cases using Equation (3) are 87.50, 57.92, 91.72 and 73.79 kJ, respectively.

Explosion energy of CO₂ blasting based on the Span and Wagner EOS

The Span and Wagner EOS is typically expressed in the form of a fundamental equation in terms of the Helmholtz free energy such as the explosion energy discussed above. The equations for the calculation of internal energy E, entropy s and speed of sound w from the dimensionless Helmholtz function can be written as

$$\frac{E(\delta, \tau)}{RT} = \tau(\emptyset_\tau^o + \emptyset_\tau^r) \tag{4}$$

$$\frac{s(\delta, \tau)}{R} = \tau(\emptyset_\tau^o + \emptyset_\tau^r) - \emptyset^o - \emptyset^r \tag{5}$$

where $\delta = \rho/\rho_c$ is the reduced density and $\tau = T_c/T$ is the reduced temperature, both normalised with their critical values, ρ_c and T_c, respectively, $\emptyset^o$ is a function for the ideal-gas behaviour and $\emptyset^r$ is a function for the residual fluid behaviour.

Based on Equations (2), (4) and (5), the energy of carbon dioxide explosion in the steel tube can be obtained as

$$\text{Energy of explosion} = \int_1^2 p\,\mathrm{d}V \cong -\Delta A \cong -(E_2 - E_1) + (T_2 s_2 - T_1 s_1) \tag{6}$$

where E_1, T_1 and s_1 are the internal energy, temperature and entropy of compressed carbon dioxide before the explosion (the pressure is the peak pressure, the temperature is the peak temperature); E_2, T_2 and s_2 are the ambient pressure into which the carbon dioxide expands (the pressure is 0.10 MPa, the temperature is 293.15 K).

The corresponding explosion energies for the four experiments calculated using Equation (6) are 142.233, 124.372, 147.723 and 136.725 kJ, respectively.

Discussion of the explosion energy of CO₂ blasting

The values calculated from Equation (6) are greater than those calculated from Equation (3). This is because the explosion energy is equal to the decrease in the internal energy of the system, $-\Delta E$. In our tests, the internal energy decrease ($-\Delta E$) of the four tests calculated by Equation (4) are 67.617, 71.339, 53.561 and 56.663 kJ, respectively. These values differ from the explosion energy calculated by Equation (3) because a constant value of 1.295 for k is used in Equation (3), while, according to Span and Wagner EOS, the value of k changes when the temperature and density change.

In addition, from Equation (3) the peak temperatures of the four tests are 1365.07, 1250, 1378.95, 1316.225 K, but from Table 1 the peak temperatures of the four tests are 364.19, 341.42, 387.46, 371.96 K, respectively. This indicates that the temperature calculated by Equation (3) may not be realistic.

Therefore, based on the discussion above, although Equation (3) is commonly used to calculate the explosion energy to assess the explosion hazard levels of the CO_2 blasting system, the results are not sufficiently accurate. On the other hand, the explosion energy of CO_2 blasting calculated by the Span and Wagner EOS plus the measured pressure in the tube

is more accurate than the results obtained by Equation (3).

In summary, using the combination of Span and Wagner's CO_2 EOS with the thermodynamics of explosion, the explosion energy in a CO_2 blasting system can be calculated more accurately. Therefore, the explosion energies of the four tests are 142.233, 124.372, 147.723 and 136.725 kJ, respectively. Using the value of 4610 J/g for TNT, the four explosions of the four tests are equivalent to explosions of 30.85, 26.98, 32.04 and 29.66 g of TNT.

Conclusions

This article presents the results of an experimental study of carbon dioxide blasting. Based on the results, the following conclusions can be drawn:

(1) The rate of temperature change increases as the initial density of CO_2 decreases and the temperature rises faster when the initial temperature is higher. The graph of temperature variations appears as a concave exponential curve initially, then rapidly increases linearly, followed by a gentle increase.

(2) The effect of the initial density of CO_2 on isochoric heat capacity appears to be significant. The smaller the initial density, the larger the peak specific heat capacity at the critical temperature. The variation of the specific isochoric heat capacity can be used to divide the temperature curve into four stages. The specific isochoric heat capacity and its rate of change determine the increasing rate of temperature.

(3) Based on the pressure curve of CO_2 blasting, the process can be divided into three stages: the pressure rise stage, the pressure release stage and the pressure recovery stage. The period of time for the pressure rise stage is about 0.026–0.086 s, and that for the pressure release stage is about 0.00018–0.00026 s. In terms of the mechanism of pressure response and phase transitions of CO_2 within the tube, the tube is initially filled with high-density fluid and low-density gas. When the heater is activated, the heat is transmitted to the CO_2 and temperature and pressure increase, causing the CO_2 to enter the supercritical state. When the internal pressure exceeds the strength of the rupture disc, the disc breaks, causing the high-pressure supercritical CO_2 to be released from the tube with a rapid depressurisation. The entire process is termed the Boiling Liquid Expanding Vapour Explosion (BLEVE).

(4) Using the Span and Wagner CO_2 EOS and the thermodynamics of explosion, the proposed method can be used to calculate the explosion energy of CO_2 blasting systems. As discussed above and demonstrated using figures measured in our experiments, the calculation results are more accurate for carbon dioxide blasting systems.

ORCID

Chaoshui Xu http://orcid.org/0000-0001-6662-3823

References

Abbasi T, Abbasi S. 2007. The boiling liquid expanding vapour explosion (BLEVE): mechanism, consequence assessment, management. *J Hazard Mater.* 141(3):489–519.

Bajpayee T, Rehak T, Mowrey G, Ingram D. 2004. Blasting injuries in surface mining with emphasis on flyrock and blast area security. *J Saf Res.* 35(1):47–57.

Caldwell T. 2004. A comparison of non-explosive rock breaking techniques. School of Engineering, The University of Queensland.

Calvignac B, Rodier E, Letourneau J-J, Almeida dos Santos PM, Fages J. 2010. Cocoa butter saturated with supercritical carbon dioxide: measurements and modelling of solubility, volumetric expansion, density and viscosity. *Int J Chem Reactor Eng.* 8(1):A73.

Campbell Sr RL. 1982. A review of methods for concrete removal. DTIC Document.

Clairet J. 1952. Use of Cardox in coal mining in Sarre. *Revue del 'Industrie Minerale.* 33:846–854.

Durga S, Swetha R. 2015. Disaster prevention and control management. *Procedia Earth Planet Sci.* 11:516–523.

Elshahomi AM. 2015. Modelling of gas decompression process for CO_2 transmission pipeline [Doctor of Philosophy thesis]. University of Wollongong.

Gaertner HJ. 1952. Application of Cardox in mining. *Glueckauf.* 87:729–738.

Guo X, Yan X, Yu J, Zhang Y, Chen S, Mahgerefteh H, Martynov S, Collard A, Proust C. 2016. Pressure response and phase transition in supercritical CO_2 releases from a large-scale pipeline. *Appl Energy.* 178:189–197.

Hawkes I. 1958. The blasting action of the Cardox shell. *Trans Inst Min Engrs.* 118:1.

Kinney GF, Graham KJ. 2013. *Explosive shocks in air.* 2nd ed. New York: Springer Science & Business Media.

Lu T, Wang Z, Yang H, Yuan P, Han Y, Sun X. 2015. Improvement of coal seam gas drainage by under-panel cross-strata stimulation using highly pressurized gas. *Int J Rock Mech Min Sci.* 77:300–312.

Mellor M. 1980. Icebreaking concepts. DTIC Document.

Mizuno H, Sawada K, Sasoh A. 2002. Numerical analysis of carbon dioxide flowfield in expansion-tube. 8th AIAA/ASME Joint Thermophysics and Heat Transfer

Conference. American Institute of Aeronautics and Astronautics.

Pantovic R, Milic V, Stojadinovic S. 2002. Consideration of possibilities for application of CARDOX method in purpose of improvement of coal fragmentation. IOC 2002: 34th International October Conference on Mining and Metallurgy.

Parsakhoo A, Lotfalian M. 2009. Demolition agent selection for rock breaking in mountain region of hyrcanian forests. *Res J Environ Sci.* 3(3):384–391.

Parsakhoo A, Lotfalian M, Hosseini SA. 2010. Forest roads planning and construction in Iranian forestry. *J Civil Eng Constr Technol.* 1(1):14–18.

Pesch R, Robertson A. 2007. Drilling and Blasting for Underground Space.

Ribovich J, Watson R. 1973. *Active list of permissible explosives and blasting devices approved before December 31, 1972. [Underground coal mines].* Bureau of Mines, Pittsburgh, PA, USA: Pittsburgh Mining and Safety Research Center.

Rustan A, Cunningham C, Fourney W, Spathis A, Simha K. 2010. *Mining and rock construction technology desk reference: rock mechanics, drilling & blasting.* Leiden: CRC Press.

Singh SP. 1998. Non-explosive applications of the PCF concept for underground excavation. *Tunnel Undergr Space Technol.* 13(3):305–311. English.

Span R, Wagner W. 1996. A new equation of state for carbon dioxide covering the fluid region from the triple-point temperature to 1100 K at pressures up to 800 MPa. *J Phys Chem Ref Data.* 25(6):1509–1596.

Vidanovic N, Ognjanovic S, Ilincic N, Ilic N, Tokalic R. 2011. Application of unconventional methods of underground premises construction in coal mines. *Tech Technol Educ Manag.* 6(4):861–865. English.

Weir P, Edwards JH. 1928. Mechanical loading and Cardox revolutionize an old mine. *Coal Age.* 33:288–290.

Wilson HH. 1954. Coal augers: development and application underground. *Trans Inst Min Eng.* 113:524–539.

Wood BF. 1973. Frozen ground implement. DTIC Document.

Zhang W, Zhang D, Wang H, Cheng J. 2015. Comprehensive technical support for high-quality anthracite production: a case study in the Xinqiao coal mine, Yongxia mining area, China. *Minerals.* 5(4):919–935.

Zou D, Panawalage S. 2001. Passive and triggered explosion barriers in underground coal mines – a literature review of recent research. CANMET Natural Resources Canada.